



Robust Aortic Valve Non-Opening Detection for Different Cardiac Conditions

*Hui-Lee Ooi, *Siew-Cheok Ng, *Einly Lim, †Robert F. Salamonsen, ‡Alberto P. Avolio, and §Nigel H. Lovell

*Department of Biomedical Engineering, University of Malaya, Kuala Lumpur, Malaysia; †Department of Epidemiology and Preventive Medicine, Monash University, Melbourne; ‡Australian School of Advanced Medicine, Macquaries University; and \$Graduate School of Biomedical Engineering, University of New South Wales, Sydney, NSW, Australia

Abstract: In recent years, extensive studies have been conducted in the area of pumping state detection for implantable rotary blood pumps. However, limited studies have focused on automatically identifying the aortic valve non-opening (ANO) state despite its importance in the development of control algorithms aiming for myocardial recovery. In the present study, we investigated the performance of 14 ANO indices derived from the pump speed waveform using four different types of classifiers, including linear discriminant analysis, logistic regression, back propagation neural network, and k-nearest neighbors (KNN).

Experimental measurements from four greyhounds, which take into consideration the variations in cardiac contractility, systemic vascular resistance, and total blood volume were used. By having only two indices, (i) the root mean square value, and (ii) the standard deviation, we were able to achieve an accuracy of 92.8% with the KNN classifier. Further increase of the number of indices to five for the KNN classifier increases the overall accuracy to 94.6%. **Key Words:** Aortic valve non-opening—Non-invasive—Ventricular assist device—Pump state detection.

Heart disease is the leading cause of death in the world by claiming 17 million lives every year (1). The World Health Organization predicted that by the year 2030, 23.6 million people will die from heart diseases (2). Due to the limited availability of donor organs and limitations in drug therapies, many ventricular assist devices (VADs) have been developed, including pulsatile VADs and continuous flow VADs or implantable rotary blood pumps (IRBPs). Among these devices, the IRBPs have become increasingly popular because of their smaller size and therefore easier implantation.

Determination of optimal speed for an IRBP is important to satisfy the varying physiological needs of a patient. Normally, the ideal state is when there is a net positive flow across both the aortic valve and the pump, known as ventricular ejection (VE) (3-6). Detrimental conditions, such as ventricular collapse. may occur due to excessive unloading of the left ventricle (LV), whereas underpumping may lead to pump backflow and inadequate perfusion (7). Several approaches have attempted to operate the pump at the highest pump speed possible before the point of LV collapses to ensure maximum end-organ perfusion (8). However, in patients with potential for myocardial recovery and weaning, partial unloading may be more beneficial to ensure optimum LV washout (9). Full unloading of the LV with the aortic valve not opening for the entire cardiac cycle has been reported to cause complications such as recirculation and stasis inside the LV cavity (10,11) as well as a ortic valve fusion (12).

Clinically, the aortic valve opening duration is measured using the M mode echocardiography while aortic flow is assessed using the pulsed Doppler ultrasound at regular intervals (i.e., every few months) after left ventricular assist device (LVAD) implantation. Studies on the identification of pumping states

doi:10.1111/aor.12220

Received July 2013; revised September 2013.

Address correspondence and reprint requests to Dr. Siew-Cheok Ng, Department of Biomedical Engineering, University of Malaya, Kuala Lumpur 50603, Malaysia. E-mail: siewcng@um.edu.my

using noninvasive parameters have mainly concentrated on suction detection, often generalizing the identified states into suction and nonsuction (3,4,6,13), leaving limited studies on identifying the aortic valve non-opening (ANO) state (3,5,14-17). These studies have proposed one (5,14,16,17) to three (15) ANO detection indices on data from animal studies (3,5,17) as well as human patients (14,15). It must be noted that although Karantonis et al. (3) proposed seven indices for suction detection, only two of them are related to ANO detection. The feasibility of the indices has been evaluated using statistics (5,14,16,17) as well as classifiers such as classification and regression tree analysis (CART) (3) and k-nearest neighbors (KNN) (15) with varying degrees of success.

Generally, the previous studies have three main shortcomings from the aspect of data, indices, and classifier. Most studies have limited data variability (3,5,14,15) which did not take into account variations in preload, afterload, cardiac contractilities, and other cardiovascular characteristics influencing the interaction of the native heart and the LVAD. This led to a simplistic approach where limited indices were tested, albeit with very promising results. With regard to classifiers, either none (5,14,16,17) or only a single classifier was tested (3). A recent study claimed to have tested multiple classifiers; however, they did not explicitly state the types of classifiers used (15).

In the present study, we attempted to evaluate the performance of 14 indices in detecting ANO, using experimental data obtained from four greyhounds, which spanned over a wide range of operating conditions. These include variations in cardiac contractility, systemic vascular resistance (afterload), and total blood volume (preload). These indices will then be classified as either the ANO or the VE state using four different classifiers, which includes linear discriminant analysis, logistic regression, back propagation neural network, and KNN. From this study, we will be able to identify which combination of indices and classifier works best in ANO detection as well as their shortcomings in ANO detection in different cardiac conditions.

MATERIALS AND METHODS

Surgical procedure

Upon performing sternal split operation and opening of the pericardium to expose the heart, diathermy and bone wax were used to obtain hemostasis (18). During the LVAD implantation procedure, the region of the aorta where the outflow graft of the pump was attached was isolated via a side-biting

clamp (18). With continuous suture method, the outflow graft was attached to the aorta as an end-to-side anastomosis after making an incision in the aortic wall (18). By using a cylindrical cutter of appropriate diameter, coring of the ventricular apex was performed and the inlet cannula was sutured to the apical myocardium (18). The pump and outflow conduit were de-aired and both of them were connected once the inlet cannula was in place (18). Small doses of potassium chloride and amiodorone were administrated to control ectopic beats (18).

This study was carried out in strict accordance with the Code of Conduct for Scientific Procedures Using Animals. The protocol was approved by the Alfred Medical Research and Education Precinct Animal Ethics Committee (AEC Approval No: E/0732/2008/m). All surgery was performed under anesthetization with propofol and isoflurane after premedication with acepromazine and atropine. Implantation of the pump was carefully executed without significant arrhythmia or blood loss. All efforts were made to minimize suffering and euthanasia was performed upon completion of experimentation.

Data acquisition

Four healthy, anesthetized, open-chest greyhounds were implanted with VentrAssist IRBP (Ventracor Ltd, Sydney, NSW, Australia). Incorporated with a third-generation centrifugal pump and novel hydrodynamic bearing that produces a characteristically flat pump-head versus pump-flow curve (5), the VAD uses apico-aortic configuration and its pump speed is controlled by a proportional integral controller with a time constant of approximately 3.5 ms (18). This allows the impeller speed to be modulated by the cardiac cycle (6). In the present study, cardiac cycle time for all subjects under various conditions ranged between 0.48 and 0.84 s (heart rate of 71 to 125 bpm), and the respiratory frequency for the ventilator was set at 12 to 14 breaths per minute.

Different pumping conditions (19) were undergone as the apex of the LV was inserted with the inflow cannula, whereas the outflow cannula was anastomosed to the ascending aorta. The greyhounds were instrumented with indwelling catheters and disposable Tru Wave pressure transducers (Edwards Life Sciences Pty Ltd., Sydney, Australia) to obtain readings of aortic pressure (AoP), inlet pressure and left ventricular pressure (LVP), left atrial pressure (LAP), vena cava pressure, pulmonary arterial pressure (PAP), pump inlet pressure (INP), and pump outlet pressure (OUP) (19). LVP was measured at the proximal part of the left ventricle and LAP was measured from the left atrium (19). OUP was measured

at the pump outflow cannula near the pump outlet whereas measurement of INP was obtained at the pump inflow cannula in proximity to the pump inlet (19). Ultrasonic flow probes (Transonics perivascular and tubing flow sensors) interfaced with the T106 flowmeter (Transonic Systems, Inc., Ithaca, NY, USA) were placed around the ascending aorta to record aortic flow rate (AoQ) and pump flow rate (18). The sampling rate of the data acquisition system was set to 4 kHz. In accordance with most noninvasive pump state detection studies, the data were down-sampled to 200 Hz (3).

Each greyhound experiment began with a speed ramp under healthy conditions and the impeller speed set point was increased in 100 rpm increments, starting from 1600 rpm. At each speed set point, the subsequent speed level was set only after all variables reached steady state. Stability is assumed to be achieved when central venous pressure and volume in the venous chamber remained unchanged for at least 20 min (18). This was then followed by various perturbations on the cardiac contractility, afterload and preload, as indicated from the low, medium, and high levels of systemic vascular resistance as well as total blood volume.

From the original healthy condition, a betaadrenergic blocking agent (metoprolol) was administrated, leading to a decrease in heart rate, cardiac contractility, and cardiac output. To induce low afterload with reduced contractility condition, injection of this drug was continued until either the baseline cardiac output reached 50% of the healthy condition, or until the aortic pressure dropped below 60 mm Hg at a speed of 1600 rpm (18). Additional afterload levels, that is, medium and high, were induced via the administration of metaraminol, which increased the mean aortic pressure by approximately 20 mm Hg at each level of afterload. The rate of the cardiotomy suction system was varied to alter the total blood volume that led to different preload levels, that is, low, medium, and high.

State identification

In the present study, the noninvasive pump speed data were used to differentiate the VE state from the ANO state. First, it was categorized into either of these states using data obtained from three different noninvasive sensors which serve as the gold standard. These include the LVP, AoP, and AoQ (5,19). The ANO state was identified based on the following three conditions: (i) maximum LVP < AoP; (ii) AoQ \approx 0; and (iii) absence of dicrotic notch in the AoP waveform (as shown from Fig. 1).

Pump speed waveform in the VE and ANO states

With increase in pump speed, pumping state shifted from the VE state into the ANO state as seen in Fig. 2. Changes in the speed amplitude can be observed, where the range of pump speed data for the VE state is generally larger compared with that for the ANO state. The shape of the speed waveform undergoes gradual changes as well. Compared with the ANO state data, the VE speed waveform exhibited a more uniform spread of speed amplitude, approximating a sinusoidal waveform shape. However, in some data, a number of missing peaks or slightly jagged peaks can be observed as the ANO state is approached. More minor irregularities started to appear as the signal transits from the VE to the ANO state. As described in previous investigations (3,5), the ANO speed waveform demonstrated missing peaks, saddles, dual peaks, or sometimes even erratic waveforms (Fig. 3).

Determination of cardiac cycle

In order to extract the cycle-based indices from the pump speed signal, determination of the cardiac cycles was first performed on the data. The raw signal was low pass filtered (10 Hz cutoff frequency) to remove high frequency, after which a moving average filter was applied. Each cycle was determined by taking the consecutive alternate intersection points between the filtered signal and the moving-averaged filtered signal (3,6).

Different values for duration of moving average have been tested (0.5, 1, and 2 s). When the waveform is irregular and the moving average size is too small, overestimation in the number of cycles occurs, causing single imperfect peaks to be misidentified as multiple cycles. In contrast, underestimation in the number of cycles occurs if the moving average size is too large, particularly in the case of baseline shift. Figure 4 illustrates the effects of different moving average size on the cycle determination. It was found that moving average size of 1 s is the most efficacious in determining the number of cycles. A total number of 10 321 cycles of ANO data and 9976 cycles of VE data were extracted from the raw data using this method.

ANO indices

In the present study, we studied 14 indices, as defined in Table 1, in which six have been used in previous studies (3,15,16), whereas the remaining indices were newly proposed in this study based on their relationship with the existing indices. These indices can be classified into five different classes. The first class was related to the range of the cycle. The

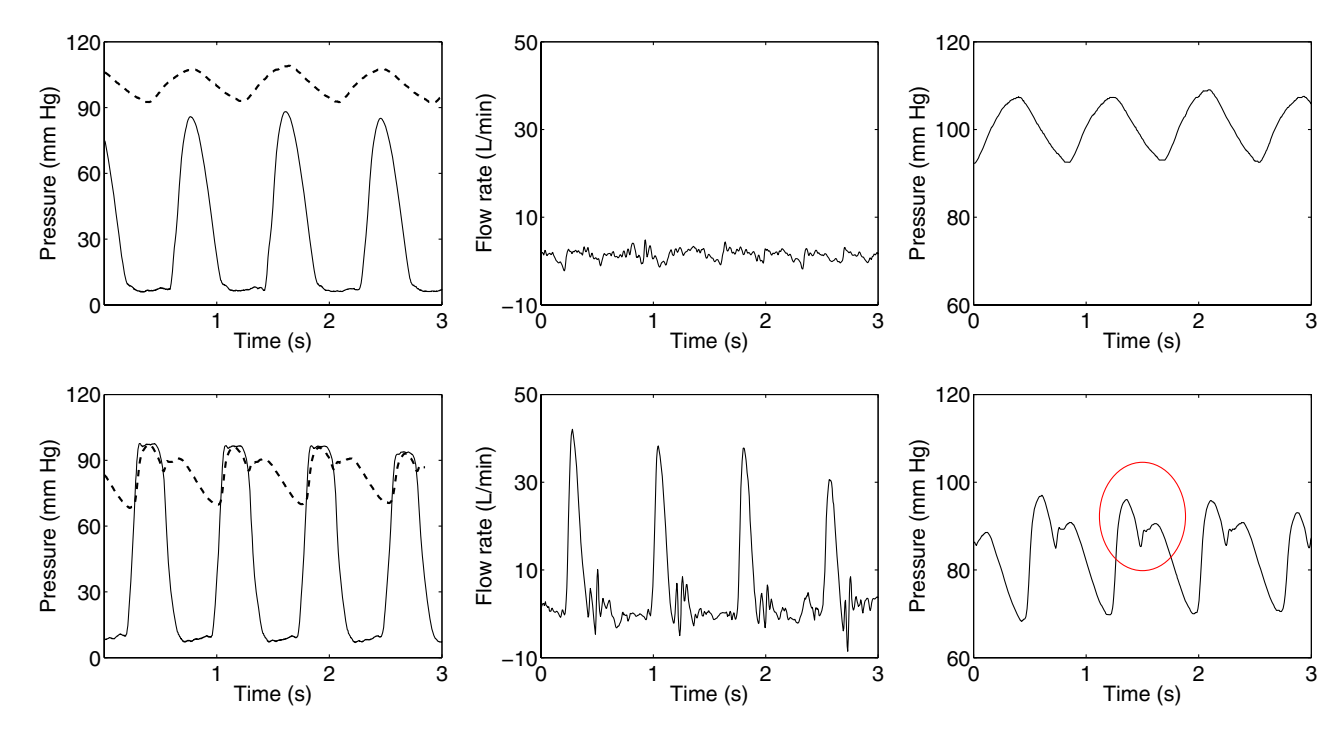


FIG. 1. Determination of pumping states (ANO, upper figures; VE, lower figures) using three different conditions as shown in the three different columns. In the first column, it can be seen that LVP (solid line) is lower than AoP (broken line) for the ANO state. In the second column, it can be seen that AoQ net flow is close to zero for the ANO state. In the third column, it can be seen that there is an absence of dicrotic notch in the AoP waveform for the ANO state.

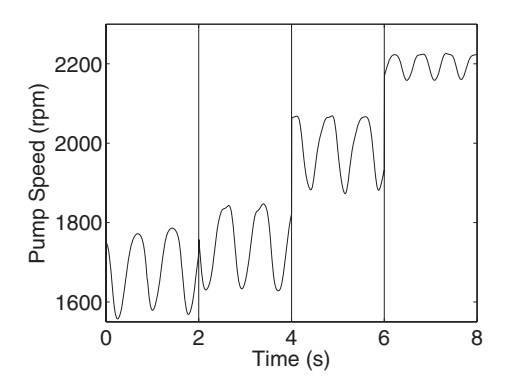


FIG. 2. Changes of state due to increase in pump speed. The first two segments show samples of the VE states while the third and fourth are samples of the ANO states.

range (Ran_1) index was selected as the ANO state has been reported to have a smaller amplitude as compared with the VE state (3). Aside from deriving the range, we proposed two additional related indices, that is, the lower range (Ran_2) as well as the upper range (Ran_3) .

The ratio of the lower range to the mean value (Dir_1) , and ratio of the upper range to the mean valve (Dir_2) , have been previously proposed by Karantonis et al. (3) and Endo et al., respectively (16,17).

The third class of indices is obtained based on the statistical properties of the data which describe the

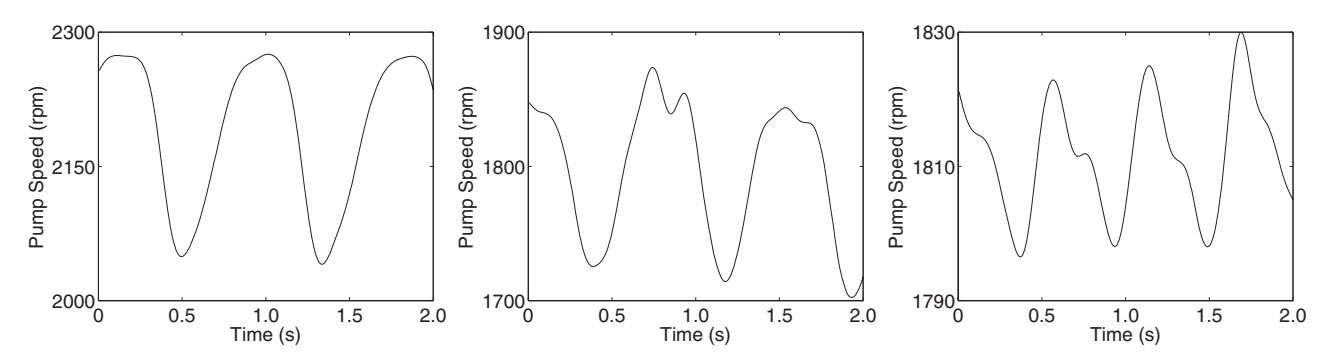


FIG. 3. Typical types of ANO pump speed waveform. The ANO waveforms have a flat plateau with sharp peaks (left), dual peak (center), as well as having saddle points (right).

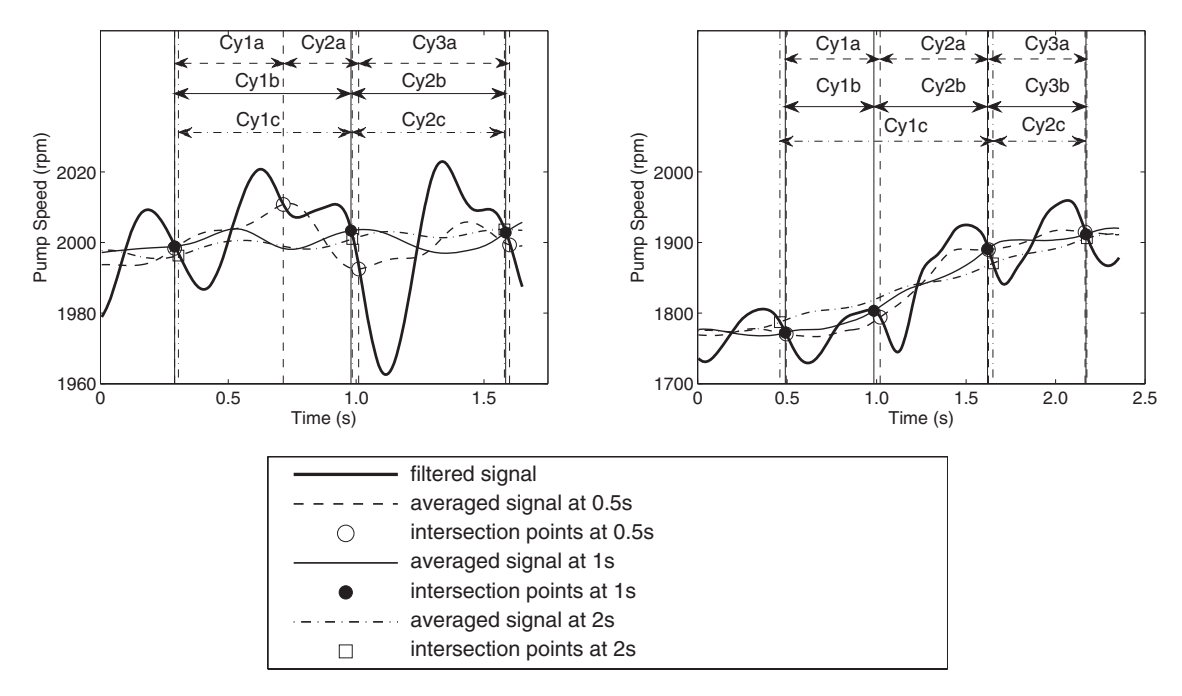


FIG. 4. Effects of moving average size on cycle determination. Cy indicates cycle while the number indicates which cycle it is. The moving average size is as follows: a = 0.5 s, b = 1 s, and c = 2 s. The left figure shows a sample of irregular waveform where the moving average size of 0.5 s overestimated the number of cycles. The right figure shows a waveform with a baseline shift where the moving average size of 2 s underestimated the number of cycles.

morphology of the speed waveform. Skewness (Sta_2) and kurtosis (Sta_3) have been used in a previous study (15). The standard deviation (Sta_1) index, which relates closely to skewness and kurtosis, was proposed in the present study.

The fourth class was derived from the root mean squared (rms) value (5,15). The crestfactor (Rms_2)

index proposed by Granegger et al. (15) was defined as the maximum value divided by the rms value. This led us to propose two other related indices, that is, the rms (Rms_1) and the minimum divided by rms (Rms_3) index

The last category of indices was proposed as minor modification to the indices in the rms category. The

TABLE 1. Description of ANO detection	on maices	S .
--	-----------	-----

Index	Description	Formula	References
Ran_1	Range	max(x) - min(x)	(3)
Ran_2	Lower range	mean(x) - min(x)	
Ran_3	Upper range	max(x) - mean(x)	
Dir_1	Range/mean	$Ran_1/mean(x)$	(16)
Dir_2	Lower range/range	Ran_2/Ran_1	(3)
		$\sqrt{(\sum (x - mean(x))^2}$	
Sta_1	Standard deviation	$\frac{\cdot}{n}$	
Sta ₂	Skewness	$\frac{\sum (x - mean(x))^3}{(n-1)Sta_1^3}$	(15)
2		* *	
Sta_3	Kurtosis	$\frac{\sum (x - mean(x))^4}{(n-1)Sta_1^4}$	(15)
51113	TKUI (USIS	$(n-1)Sta_1^4$	(13)
Rms_1	Root mean square	$\sqrt{mean(x^2)}$	
Rms_2	Maximum/rms	$max(x)/Rms_1$	(15)
Rms_3	Minimum/rms	$min(x)/Rms_1$	()
Rmr_1	Root mean and range	$\sqrt{mean(x) \times Ran_1}$	
Rmr_2	Maximum/rmr	$max(x)/Rmr_1$	
Rmr_3	Minimum/rmr	$min(x)/Rmr_1$	

x represents the data within a cycle of pump speed.

rms value (Rms_1) was replaced by having the square root of multiplication from the mean and the range (Ran_1) to give (Rmr_1) , the maximum value divided by (Rmr_1) to give (Rmr_2) and the minimum value divided by (Rmr_1) to give (Rmr_3) .

Classification techniques

Two main types of supervised classifiers are available: (i) the parametric classifiers, where the data distribution is assumed to be normal; and (ii) the nonparametric classifiers, which do not make any assumptions on the data distribution. In this study, two parametric classifiers, namely linear discriminant analysis (LDA) (13) and logistic regression (LR) (6), as well as two nonparametric classifiers consisting of the back-propagation neural network (BPNN) (4) and KNN (15) were applied to the data.

Linear discriminant analysis finds a set of weights that form a linear decision boundary based on the distribution of the different classes. LDA maximizes class discrimination by taking into consideration the between-class variance and within-class variance. Linear discriminant coefficient was thus produced and probability of each test data being in a particular class was calculated. This method does not require any testing to find the optimal parameters. In spite of this, many studies have shown that LDA performance is comparable, if not better than other more advanced classifiers (20,21).

LR finds a set of coefficients for the best fitting function by minimizing cost function via gradient descent. A regularization parameter, α is used in order to prevent the problem of overfitting resulting from the usage of multiple indices. In the present study, we chose $\alpha = 0.01$ as its performance was similar to all other tested values ($\alpha = 0.01, 0.02, 0.05, 0.1, 0.5, and 1$).

For the BPNN algorithm, error reduction in predicting the data set is done through iterative changes to the network of nodes. Computation of cost function in an iterative manner takes into account the number of hidden nodes, number of hidden layers, as well as learning rate. The number of hidden nodes plays a major role in determining the success of the BPNN as too many nodes may result in overlearning while too few nodes may result in insufficient ability to learn. Hidden nodes of sizes 1, 2, 3, 5, and 10 were tested. However, different learning rates (i.e., 0.1, 0.03, 0.01, 0.003, and 0.001), which play an important role in determining whether the network could approach the optimal minima, were tested. From our study, we found that two hidden nodes with a learning rate of 0.01 gives reliable performance.

Also known as nonparametric lazy learning algorithm, the KNN approach classifies an object by majority vote of its neighbors. No explicit training of data is involved for this technique and the training data are only used during the testing phase. The indices are first normalized before the Euclidean distance is used as a similarity measure to determine their respective surrounding neighbors. The number of neighbors, k, significantly affects the performance of the classifier. A low k value may render the test result highly susceptible to noise, while a high k value may unnecessarily include points from other classes (22). It was observed from our study that the value of k required for optimal performance increases with the addition of indices. By taking into consideration such phenomenon, different k values (odd numbers from 3 until 41) were heuristically tested with cross-validation and k = 23 was finally chosen.

During the implementation of all the classification methods, a ten-fold cross validation was applied. The average of the statistical measures from each of these was taken to represent the classification performance.

Experimental studies

Two experimental studies were performed. For the first study, we attempted to determine the performance of the individual indices using the different types of classifiers, in terms of sensitivity and specificity.

In the second experimental study, we attempted to find the best combination of indices for the four different types of classifiers using the sequential forward floating selection (SFFS) method. Because we found that different classifiers resulted in different sets of optimal index combinations using the SFFS method, we further performed a comprehensive study on the performance of all possible combinations of two indices on all the classifiers, resulting in a total of 364 combinations. Results showed that there are some discrepancies in the two best indices given by SFFS compared with that provided by the exhaustive search on all possible combinations. Consequently, to search for the best combination of more than two indices, we applied SFFS starting from the best combination of two indices provided by the exhaustive search.

RESULTS

Table 2 shows the performance of the individual ANO detection index obtained from the four different classifiers, expressed in terms of sensitivity, specificity, and overall accuracy. In general, most of the

LDA **BPNN** KNN LR Ran_1 68.0/50.3 (59.3) 67.6/51.1 (59.5) 47.9/97.2 (72.1) 60.1/86.5 (73.0) 66.4/54.7 (60.6) Ran_2 66.2/55.4 (60.9) 47.3/96.4 (71.5) 56.0/86.5 (71.0) 68.6/47.2 (58.1) 68.3/48.3 (58.5) Ran_3 49.3/95.1 (71.8) 61.4/85.0 (73.0) 56.5/95.5 (75.7) 60.5/90.1 (75.1) Dir_1 73.4/62.6 (68.1) 72.7/64.1 (68.5) 62.5/54.8 (58.7) 62.6/54.6 (58.7) 57.3/56.1 (56.7) Dir_2 51.1/65.6 (58.2) 68.0/51.5 (59.9) 68.7/50.5 (59.7) 50.8/97.1 (73.5) Sta_1 62.6/86.2 (74.2) 63.4/50.8 (57.2) 63.3/50.8 (57.2) 51.1/64.8 (57.9) 58.2/57.0 (57.6) Stan 66.5/60.5 (63.5) 58.2/68.9 (63.5) 66.0/58.6 (62.4) Staz 60.4/66.8 (63.6) Rms_1 55.9/93.1 (74.2) 56.8/91.1 (73.7) 61.2/82.4 (71.5) 63.4/85.8 (74.4) Rms_2 0.0/100.0 (49.1) 70.6/67.0 (68.8) 58.1/90.6 (74.1) 58.7/89.6 (73.9) 0.0/100.0 (49.1) 57.5/93.6 (75.3) 61.3/88.6 (74.7) Rms_3 73.1/61.4 (67.4) Rmr_1 63.3/44.1 (53.9) 63.3/44.4 (54.0) 44.9/95.6 (69.8) 67.7/82.4 (74.9) 60.4/90.5 (75.2) 58.8/91.7 (75.0) 65.7/76.5 (71.0) 54.8/97.5 (75.8) Rmr_2 Rmr_3 59.3/90.7 (74.7) 65.8/76.2 (70.9) 54.8/97.5 (75.8) 60.3/90.1 (75.0) ≥70% 3 3 10 11

TABLE 2. Performance of the 14 individual indices using the four different classifiers

The results are shown as sensitivity/specificity (overall accuracy). The last row indicates the number of individual indices that achieve accuracy of 70% and above for each classifier.

indices could achieve an accuracy of more than 70% when used individually. In spite of this, the accuracy was heavily skewed toward VE state.

The performance of the classifiers was evaluated with regard to the following aspects: (i) total number of indices with an overall accuracy exceeding 70%; and (ii) total number of indices with both sensitivity and specificity exceeding 65%. Based on the first criteria, KNN was the best classifier, with 11 indices achieving an accuracy above 70%, followed by BPNN (10), LDA and LR (3 each). LR achieved the best performance in terms of balanced sensitivity/ specificity, with three indices achieving both sensitivity and specificity above 65%, followed by KNN (1). Both BPNN and LDA did not have any index which fulfilled this criteria.

The performance of the individual indices was assessed from two aspects: (i) the best possible accu-

91.1

87.6

89.3

89.4

2

77.7

91.5

76.2

76.2

4

77.7

78.0

77.3

77.3

89.2

91.6

91.6

91.6

5

83.1

87.9

86.6

86.7

1

87.9

91.2

91.0

91.0

5

Rms3

 Rmr_1

 Rmr_2

 Rmr_3

>90%

racy from any classifier; and (ii) robustness with respect to their accuracy across different classifiers. With regard to the first aspect, Rmr_2 and Rmr_3 outperformed other indices with accuracy of 75.8%, followed by Dir_1 (75.7%) and Rmr_1 (74.9%). Rms_1 , Rmr_2 , and Rmr_3 are the most robust, with accuracy of more than 70% from all the four classifiers. Dir_2 , Sta_2 , and Sta_3 were unable to achieve 70% accuracy with any classifier.

Table 3 shows the best performance for all paired combinations of indices obtained from the four different classifiers, expressed in terms of accuracy. The best performance was achieved using Rms_1 and Sta_1 , with an accuracy of 92.8% and a sensitivity/specificity of 90.0%/95.8%. Considering that the acceptable performance is at least 90% accuracy, a total number of 24 different combinations of two indices can be used. Among all indices, Rms_1 can be considered as the

Index	Ran_1	Ran_2	Ran_3	Dir_1	Dir_2	Sta_1	Sta_2	Sta_3	Rms_1	Rms_2	Rms_3	Rmr_1	Rmr_2	Rmr_3
Ran_1	_	76.4	76.2	91.2	76.6	76.9	77.4	76.8	92.0	87.4	87.9	91.2	91.0	91.0
Ran_2	76.4	_	76.5	86.9	76.7	77.2	77.3	75.3	90.8	90.0	83.1	87.9	86.6	86.7
Ran_3	76.2	76.5	_	89.1	76.8	77.4	77.6	77.3	92.0	85.5	91.1	87.6	89.3	89.4
Dir_1	91.2	86.9	89.1	_	77.5	91.8	78.2	78.2	92.1	77.5	77.7	91.5	76.2	76.2
Dir_2	76.6	76.7	76.8	77.5	_	77.6	63.2	66.0	78.5	77.7	77.7	78.0	77.3	77.3
Sta_1	76.9	77.2	77.4	91.8	77.6	_	78.3	77.1	92.8	87.9	89.2	91.6	91.6	91.6
Sta_2	77.4	77.3	77.6	78.2	63.2	78.3	_	67.0	78.7	78.0	78.4	79.0	78.2	78.1
Sta_3	76.8	75.3	77.3	78.2	66.0	77.1	67.0	_	80.0	76.2	78.5	80.0	78.2	78.4
Rms_1	92.0	90.8	92.0	92.1	78.5	92.8	78.7	80.0	_	90.7	91.8	92.1	92.1	92.1
Rms_2	87.4	90.0	85.5	77.5	77.7	87.9	78.0	76.2	90.7	_	77.8	90.2	77.7	77.8

91.8

92.1

92.1

92.1

10

77.8

90.2

77.7

77.8

2

90.2

77.7

77.8

3

TABLE 3. The performance of combinations of two indices

The highest classification accuracy among the compared classifiers for each combination is displayed. The last row indicates the number of combination sets that exceed 90% accuracy.

78.4

79.0

78.2

78.1

0

78.5

80.0

78.2

78.4

0

77 7

91.4

75.8

4

77.8

91.4

75.8

4

90.2

91.4

91.4

8

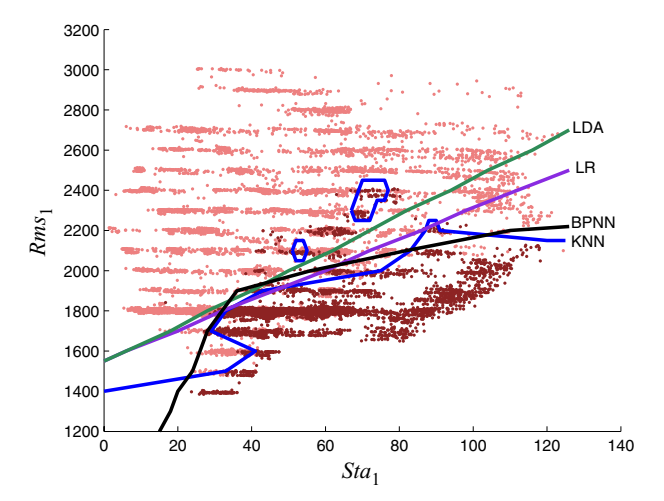


FIG. 5. The decision boundaries of the four classifiers in separating the two states using two indices (Rms_1 and Sta_1). The dark dots represent the VE condition while the light dots represent the ANO condition. The different colored lines refer to the decision boundary from the different classifiers.

best index to pair with as there are 10 combinations involving Rms_1 which could achieve an accuracy above 90%. This is followed by Rmr_1 (8), Sta_1 (5), and Ran_1 (5). The three indices which performed poorly individually, that is, Dir_2 , Sta_2 , and Sta_3 , also did not perform well in the presence of multiple indices, where none of their combination with other indices achieved an accuracy exceeding 90%.

Figure 5 shows the decision boundaries of the four classifiers in separating the ANO state from the VE state. The decision boundaries formed by the four classifiers are different from one another. The parametric classifiers (LDA and LR) formed straight lines while the nonparametric classifiers have jagged lines, which serve to optimize the classification task.

Table 4 shows the performance of the four different classifiers with increasing number of indices selected using the SFFS. With multiple indices, KNN outperformed other classifiers, where it achieved a sensitivity/specificity (overall accuracy) of 90.0%/95.8% (92.8%) with only two indices. Further increase in the number of indices for the KNN classifier increases the overall performance (sensitivity/specificity [overall accuracy] of 92.6%/96.7% [94.6%] with five indices). BPNN and LR have comparable performance when two indices are included in the classification process, but both of them showed negligible increase in performance with further increase in the total number of indices.

Table 5 compares the training as well as implementation time for the four different classifiers. Among all classifiers, only KNN is free of training. LDA has the fastest training time of $4.69\times10^{-3}\,\mathrm{s}$ for an

FABLE 4. Best combinations of indices in terms of overall accuracy for the four different classifiers

Classifier			LDA					LR					BPNN					KNN		
Indices	1	2	3	4	5	1	2	3	4	S		2	3	4	5		2	3	4	5
Ran ₁		×	×	×	×				×	×								×	×	
Ran ₃																		*	4	
Dir_1		×	×	×	×															
Dir_2																				
$\widetilde{S}ta_1$				×	×		×	×	×			×	×	×	×		×	×		;
Sta_2																				×
Sta_3			×		×					×					×				×	×
Rms_1						×	×	×	×	×		×	×	×	×		×	×	×	×
Rms_2														×	×					×
Rms_3								×	×	×			×	×	×				×	×
Rmr_1				×	×					×										
Rmr_2	×															×				
Rmr_3											×									
Accuracy	75.0	88.2	89.7	0.06	90.1	73.7	8.68	6.68	0.06	90.2	75.8	8.06	8.06	2.06	8.06	75.2	92.8	93.8	94.3	94.6

Second row indicates the number of indices used. X indicates the presence of the specified index in the combination sets with respect to each classifier. The last row shows the accuracy obtained from the corresponding index combination sets as indicated in each column

TABLE 5. Comparison of training and implementation time for different classifiers

	Training	time (s)	Implementa	tion time (s)
Classifier	1 index	2 indices	1 index	2 indices
LDA LR BPNN KNN	4.69×10^{-3} 1.06×10^{-1} 7.28×10 0	8.25×10^{-3} 3.70 8.93×10 0	1.42×10^{-4} 7.85×10^{-5} 1.02×10^{-4} 9.68×10^{-1}	$1.51 \times 10^{-4} \\ 8.61 \times 10^{-5} \\ 1.10 \times 10^{-4} \\ 1.10$

individual index and 8.25×10^{-3} s when two indices are used, followed by LR, which requires 1.06×10^{-1} s for an individual index and 3.70 s for two indices. BPNN, which involves multiple iterations before the network is trained, requires 72.8 s for an individual index and 89.3 s for two indices. With regard to implementation time, KNN is the slowest, with 9.68×10^{-1} s for an individual index and 1.1 s for two indices. All the three remaining classifiers have very short implementation time in the range of 1×10^{-4} for one or two indices.

DISCUSSION

With increasing evidence showing successful experience for prolonged periods of IRBP implantation (23), much focus has been put on developing physiologically responsive pump control strategies which could promote myocardial recovery and subsequent weaning of the IRBP patients. In patients with the potential for myocardial recovery, partial unloading, to minimize the risk of LV stasis and aortic valve fusion, has been suggested to be more beneficial as compared with full unloading (9). In order to achieve such a control strategy, it is imperative to reliably and accurately differentiate various physiologically significant pumping states for any IRBP.

Despite extensive research in the field of pumping state detection (3,5,14-17), a limited number of studies have been conducted to automatically differentiate ANO from the VE state. In one of the earliest studies performed on three acute ovine models. Avre et al. (5) proposed the state transition index, defined as the ratio of the difference in the maximum minus the rms value to the difference in the mean speed between two successive cycles to be a good index for ANO detection. In another study, Endo et al. (16,17) found that the index of motor current amplitude (equivalent to Dir_1), calculated as the ratio of the current amplitude to the mean current, was able to detect the transition point between partial assist and full assist. Although *Dir*₁ performed reasonably well in the present study with an accuracy of 75.7% individually, its absolute value was shown to be highly dependent on cardiac contractility and afterload (16), thus affecting intersubject robustness. Although these studies provide a platform for further research, they have a common limitation where no automated system for classification was provided and thus a statistical basis for comparison could not be made (3).

In order to account for the large variations in the waveform patterns, Karantonis et al. (3) and Granegger et al. (15) have proposed methods using a combination of several indices. Employing a CART on six ex vivo porcine experiments using the VentrAssist pump (same model as the present study), Karantonis et al. reported a specificity/sensitivity of 100%/100% in detecting the ANO state. However, the two indices used in their study which were related to the ANO state, that is, Ran_1 and Dir_2 , could only achieve an accuracy of 73.2 and 58.7% respectively, in the present study when applied individually, and an accuracy of 76.6% when combined together. The main reason behind the large discrepancy between their reported performance and our results is that their experimental measurements, obtained from healthy pigs, have limited data variability. We found from our results that whereas Dir₂ performed poorly in all scenarios, the absolute value of Ran_1 was substantially affected by different physiological conditions. This revealed that different levels of perturbations in the cardiovascular system (such as systemic vascular resistance and contractility) need to be taken into consideration in the experiments to ensure robustness of the classification approach.

Based on their visual observation of the pump flow signal, Granegger et al. (15) proposed three indices for ANO detection, namely skewness (Sta2), kurtosis (Sta_3), and crest factor (Rms_2). The combination of indices was implemented with a KNN approach using both a numerical model and animal experiments, and resulted in an accuracy of 95%. However, when the same indices were applied on the pump speed data in the present study, we could only achieve an accuracy of 84.3%. Interestingly, while Sta₂ and Sta₃ (which describe the morphology of a particular waveform) showed relatively poorer performance when compared with other indices, their close counterpart from the same class, that is, Sta_1 proposed in the present study, performed reasonably well both individually as well as in combination with other indices. The difference in performance using the same indices on two different sets of data may be caused by a difference in the type of waveforms (flow signal vs. speed signal) or pump models (axial vs. centrifugal). For example, crest factor (*Rms*₂) proposed by Granegger et al. (15) may be more sensitive to changes in waveform closer to the x-axis such as pump flow, than that with relatively higher magnitudes such as pump speed. The main drawback of their study is the use of invasive flow sensors, which may affect system reliability and increase cost.

With regard to the performance of classifiers, the present study showed that KNN outperformed other classifiers, particularly with an increasing number of indices. This is consistent with the findings by Granegger et al. (15) who claimed to have evaluated multiple classifiers, although it is unclear which types of classifiers were tested in their study. Generally, the parametric classifiers (LDA and LR) have short training (less than a few seconds) and implementation time (in the range of 10⁻⁴ s). In contrast, BPNN has comparable implementation time but long training time (80 s).

Despite the high accuracy of KNN, the implementation time of this classifier, approximately 1 s, is comparatively longer than other classification techniques applied in this study. Although ideally it is desirable to have single beat classification in real time, common medical experience with human subjects assisted by rotary VAD (Dr. Robert Salamonsen, The Alfred Hospital, Melbourne, Australia) indicates that an estimate of valve opening at every 5 to 10 heart beats is sufficient. This is evident in clinical observation (12) that reported that duration of the device placement of four subjects with partial aortic valve fusion ranges from 26 to 689 days. In another further study conducted in 17 VAD-treated patients (24), commissural fusion of aortic valves of varying degree were found in implantation that ranges from 4 to 787 days. ANO occurrence is a gradual process and hence having a multiple beat system as opposed to single beat classification does not critically affect its overall effectiveness.

It was observed that for all the tested classifiers, there is a portion of data that misclassifies consistently. Further investigation has revealed that the false negative originated from a particular subject with exceptionally high systemic peripheral resistance. This has affected the amplitude range and mean pump speed data, thereby influencing the performance of the proposed index combination. As compared with other subjects, the transition threshold from VE to ANO state for this subject was greatly increased. Data of VE state in the subject were mistakenly classified as ANO state during the study, thus decreasing the overall performance of ANO detection algorithm.

CONCLUSION

In this study, we have tested 14 aortic valve nonopening indices using four different types of classifiers on 10 321 cycles of ANO data and 9976 cycles of ventricular ejection data, over a wide range of cardio-vascular system operating conditions. Using only two indices, (i) the root mean square value, and (ii) the standard deviation, we were able to achieve an accuracy of 92.8% with the KNN classifier. A further increase of the number of indices to five for the KNN classifier increases the overall accuracy to 94.6%.

Acknowledgments: The authors would like to thank the Ministry of Higher Education Malaysia (grant number: UM/HIR (MOHE)/ENG/50) and the Australian Research Council Linkages scheme for providing the research grant support.

REFERENCES

- McKay J, Mensah GA, Greenlund K. The Atlas of Heart Disease and Stroke. Geneva: World Health Organization, 2004.
- Mendis S, Puska P, Norrving B, et al. Global Atlas on Cardiovascular Disease Prevention and Control. Geneva: World Health Organization, 2011.
- Karantonis DM, Lovell NH, Ayre PJ, Mason DG, Cloherty SL. Identification and classification of physiologically significant pumping states in an implantable rotary blood pump. Artif Organs 2006;30:671–9.
- Karantonis DM, Cloherty SL, Lovell NH, Mason DG, Salamonsen RF, Ayre PJ. Noninvasive detection of suction in an implantable rotary blood pump using neural networks. *Int J Comput Intell Appl* 2008;7:237–47.
- Ayre P, Lovell N, Morris R, Wilson M, Woodard J. Identifying physiologically significant pumping state transitions in implantable rotary blood pumps used as left ventricular assist devices: an in-vivo study. In: Engineering in Medicine and Biology Society. Proceedings of the 25th Annual International Conference of the IEEE. 2003.
- Ng S-C, Lim E, Mason DG, Avolio AP, Lovell NH. Evaluation of suction detection during different pumping states in an implantable rotary blood pump. *Artif Organs* 2013;37:145–54.
- Yi W. Physiological control of rotary left ventricular assist device. In: Control Conference, 2007. CCC 2007. Chinese. IEEE. 2007; 469–74.
- Gwak K-W, Antaki JF, Paden BE, Kang B. Safety-enhanced optimal control of turbodynamic blood pumps. *Artif Organs* 2011;35:725–32.
- Andrade JG, Al-Saloos H, Jeewa A, Sandor GG, Cheung A. Facilitated cardiac recovery in fulminant myocarditis: pediatric use of the Impella LP 5.0 pump. J Heart Lung Transplant 2010;29:96–7.
- Lazar RM, Shapiro PA, Jaski BE, et al. Neurological events during long-term mechanical circulatory support for heart failure: the randomized evaluation of mechanical assistance for the treatment of congestive heart failure (rematch) experience. Circulation 2004;109:2423–7.
- Rose AG, Park SJ. Pathology in patients with ventricular assist devices: a study of 21 autopsies, 24 ventricular apical core biopsies and 24 explanted hearts. *Cardiovasc Pathol* 2005;14:19–23.
- Rose AG, Park SJ, Bank AJ, Miller LW. Partial aortic valve fusion induced by left ventricular assist device. *Ann Thorac* Surg 2000;70:1270–4.
- Ferreira A, Chen S, Simaan MA, Boston JR, Antaki JF. A discriminant-analysis-based suction detection system for rotary blood pumps. In: Engineering in Medicine and Biology Society, 2006. EMBS'06. 28th Annual International Conference of the IEEE. 2006; 5382–5.

- Bishop CJ, Mason NO, Kfoury AG, et al. A novel non-invasive method to assess aortic valve opening in HeartMate II left ventricular assist device patients using a modified Karhunen-Loève transformation. J Heart Lung Transplant 2010;29:27– 31.
- Granegger M, Moscato F, Mahr S, Wieselthaler G, Schima H. Assessment of the aortic valve opening during rotary blood pump support. ASAIO J 2011;57:75.
- Endo G, Araki K, Kojima K, Nakamura K, Matsuzaki Y, Onitsuka T. The index of motor current amplitude has feasibility in control for continuous flow pumps and evaluation of left ventricular function. *Artif Organs* 2001;25:697–702.
- Endo G, Kojima K, Nakamura K, Matsuzaki Y, Onitsuka T. The meaning of the turning point of the index of motor current amplitude curve in controlling a continuous flow pump or evaluation of left ventricular function. *Artif Organs* 2003;27:272-6.
- Lim E. Characterisation of cardiovascular-rotary blood pump interaction. PhD dissertation, Graduate School of Biomedical Engineering, The University of New South Wales (UNSW), Sydney, Australia, 2010.
- Lim E, Dokos S, Salamonsen RF, Rosenfeldt FL, Ayre PJ, Lovell NH. Numerical optimization studies of

- cardiovascular-rotary blood pump interaction. *Artif Organs* 2012;36:E110-24.
- Mohamadi Monavar H, Afseth N, Lozano J, Alimardani R, Omid M, Wold J. Determining quality of caviar from Caspian Sea based on Raman spectroscopy and using artificial neural networks. *Talanta* 2013;11:98–104.
- Liu P. Feature extraction for identification of drug and explosive concealed by body packing based on discrete cosine transform plus linear discriminant analysis. *Anal Methods* 2013;5:1935–40.
- Johansson U, Boström H, König R. Extending nearest neighbor classification with spheres of confidence. Proceedings of the 21st Florida Artificial Intelligence Research Society Conference, 2008: 282–7.
- Park SJ, Tector A, Piccioni W, et al. Left ventricular assist devices as destination therapy: a new look at survival. *J Thorac Cardiovasc Surg* 2005;129:9–17.
- Connelly JH, Abrams J, Klima T, Vaughn WK, Frazier O. Acquired commissural fusion of aortic valves in patients with left ventricular assist devices. *J Heart Lung Transplant* 2003;22:1291–5. [Online]. Available at: http://www.sciencedirect.com/science/article/pii/S1053249803000287. Accessed November 10, 2013.